J. A. Sward[1]
Department of Mechanical Engineering,
University of New Mexico,
Albuquerque, NM 87131

P. C. Scott
Department of Mechanical Engineering,
University of New Mexico,
Albuquerque, NM 87131

P. J. Wayne
Department of Mechanical Engineering,
University of New Mexico,
Albuquerque, NM 87131

N. Jackson
Department of Mechanical Engineering,
University of New Mexico,
Albuquerque, NM 87131

P. Vorobieff
Mem. ASME
Department of Mechanical Engineering,
University of New Mexico,
Albuquerque, NM 87131

R. Lumia
Department of Mechanical Engineering,
University of New Mexico,
Albuquerque, NM 87131

S. V. Poroseva
Mem. ASME
Department of Mechanical Engineering,
University of New Mexico,
Albuquerque, NM 87131
e-mail: poroseva@unm.edu

Harvesting Energy From an Ionic Polymer–Metal Composite in a Steady Air Flow

The paper presents the results of an investigation of a possibility for energy harvesting from a flexible material such as an ionic polymer–metal composite (IPMC) placed in a steady flow of air characteristic of conditions typical to a densely urbanized area. As electro-active devices require dynamic loading to produce current, their response is usually evaluated in unsteady and turbulent flows, where an electro-active polymer follows the movement of the medium surrounding the device. In our study, we examine the flow conditions at which flutter sets the IPMC strip in motion. Although flutter is often perceived as an unfavorable phenomenon for aerodynamic applications and civil structures, it may be beneficial for harvesting wind energy. Of particular interest is that this phenomenon may occur in a steady flow, which potentially expands the range of favorable flow conditions for energy harvesting. In the paper, the air speed at which flutter occurs and the speed range at which flutter is sustained are provided along with the estimated amount of power produced in an IPMC sample of specified dimensions.
[DOI: 10.1115/1.4046801]

Keywords: wind energy, flutter, IPMC

1 Introduction

Ionic polymer–metal composites (IPMCs) have been the subject of an increasing amount of research recently due to their sensing and actuation capabilities. Early contributions in their manufacturing, modeling, and associated industrial and medical applications can be found in Refs. [1–4]. Many more specific modeling applications of IPMCs (and other electro-active devices) are discussed in Refs. [5–11].

Ionic polymer–metal composites consist of a thin semipermeable polymer membrane sandwiched between thin layers of metal which serve as electrodes. Cations are crosslinked to the polymer chains and are immobile when dry. When hydrated, water molecules surround the cations, rendering them mobile. When stimulated with electricity, the cations in a hydrated polymer move toward the cathode, which causes the polymer to expand toward the cathode. When subjected to mechanical deformation, a density differential develops in the polymer as a result. The hydrated cations move from the higher density to the lower density regions, creating an electric charge, which can then be conducted away via the electrodes [12]. Further detail about the mechanoelectric properties of IPMCs is found in Sec. 2.1 of this paper.

Of interest for this study is the ability of an IPMC to act as a mechanoelectric energy harvester, which converts ambient vibrational energy into electricity. The IPMC capabilities for such an application were investigated in Ref. [13], where it was found that the maximum power output of 3×10^{-9} W could be achieved with the maximum IPMC strain of 0.3% at the vibrating frequency of 7.09 rad/s (1.13 Hz). Properties of IPMCs when used as a mechanoelectric energy harvester were also reported by Tiwari and Kim [14], who showed that IPMCs could be used to harvest energy from vibrational frequencies below 50 Hz. Power density determined in Ref. [14] was $\sim$45 W/m^3.

Numerous studies were conducted to evaluate a potential for energy harvesting with IPMCs in various configurations. In Ref. [15], for example, energy exchange between a vortex ring and an IPMC was investigated. A rate of conversion from strain energy to electrical energy was found to be in the range of 0.0003–0.0012%. Aureli et al. [16] studied energy harvesting from the base excitation of IPMC and observed the maximum power generation of 1×10^{-9} W for the base excitation of 10^{-3} m. Applying a mathematical model for the chemo-mechano-electric response of an IPMC, they experimentally verified that energy harvesting is optimized when shunting on the energy harvesting circuit matches the internal resistance of IPMC. The effects of geometry and physical properties on the IPMC

[1]Present address: Sibley School of Mechanical and Aerospace Engineering, Cornell University, Ithaca, NY 14853.

Contributed by the Fluids Engineering Division of ASME for publication in the Journal of Fluids Engineering. Manuscript received August 15, 2019; final manuscript received March 20, 2020; published online April 24, 2020. Assoc. Editor: M'hamed Boutaous.

capacitance were analyzed in Ref. [17]. Cellini et al. [18] reported that power gleaned from fluid-induced buckling of IPMC was in the range of 10^{-12} to 10^{-9} W with the flow speed varying from 0.23 to 0.54 m/s. In particular, power up to a few nanowatts was harvested from a turbine composed partially of IPMCs immersed in a flow at 0.43 m/s [18,19]. Cha et al. [20] created a carangiform swimmer, whose tail mimicked that of a thresher shark, with IPMCs incorporated into the tail. They also found that the energy harvesting was maximized when the shunting resistance of an energy harvesting circuit matched the internal resistance of IPMC. Research efforts have also been devoted to construct efficient energy harvesting circuits using IPMCs [21–24] that utilize the knowledge that the IPMC energy harvesting capabilities are maximized when the shunting resistance of an energy harvesting circuit matches the internal resistance of IPMC.

The effects of aeroelastic instabilities on the energy harvesting capabilities and various geometries of electro-active materials were investigated in Refs. [25–30]. Sirohi and Mahadik designed a piezoelectric wind energy harvester that generated more than 50×10^{-3} W at a wind speed of 5.19 m/s [31]. The design used galloping of a bar with triangular cross section attached to a cantilever beam. Among the reasons their device produced that amount of power are the device dimensions and the use of piezoelectric sheets of PSI-5H4E, which has a higher energy density than IPMCs. Giacomello and Porfiri used underwater flutter of a heavy flag hosting IPMCs to harvest energy [32]. They recorded the generated power to be $\sim 10^{-10}$ W in the range of the mean flow velocities from 0.6 to 1.1 m/s. Hobeck and Inman used an array of piezoceramic wafers excited by spring steel cantilevers made to resemble blades of grass to harvest up to 10^{-3} W per sample. In another experiment, they used a similar array of mylar-coated piezopolymer cantilevers to harvest up to 1.4×10^{-6} W per sample [33]. Fei and Wen harvested up to 1.3×10^{-3} W with a stretched thin polymer belt. Airflow perpendicular to the belt then induced flutter. The resulting vibrational energy was transferred to magnets which induced current in a solenoid [34]. Perez et al. used airflow to induce flutter in a thin Teflon membrane confined between two parallel walls backed with metal electrodes. The vibration of the membrane against the walls caused a variable capacitance and a triboelectric effect resulting in an output of close to $2\,\mathrm{W/m^{-2}}$ [35]. Similarly, Ravichandran et al. placed a thin film inside of an electrode-lined venturi tube. The low pressure in the throat of the tube caused the film to flutter at high frequencies. With a film made of polycarbonate and electrodes composed of polytetrafluoroethylene and copper, the resultant triboelectric effect produced a peak power of 4.5×10^{-3} W [36]. Of interest for this study is flutter, a physical phenomenon that naturally occurs in fluid–structure interactions, and the possibility of energy extraction directly from IPMCs interacting with air using this phenomenon. Here, it must be mentioned that the history of studies of aeroelastic flutter is quite long, starting with the seminal 1930s work [37], and for a large fraction of that history, flutter was considered as the instability of a lifting surface (wing, wing with aileron, turbine blade, etc.) in a moving flow, where a positive feedback loop may arise between the deflection of the lifting surface and the aerodynamic force exerted by the flow. While the original motivation for the studies of flutter was to prevent it (and keep the lifting surfaces attached to the aircraft), flutter in its literal aeroelastic definition has also recently attracted the attention of researchers as a mechanism suitable for energy harvesting. A recent example is a flutter-driven oscillatory windmill proposed by Farthing [38]. Some of the other relevant studies on flutter of a rectangular plate are Refs. [39–46].

This paper presents the results of an investigation of the wind energy harvesting capabilities of a stand-alone rectangular IPMC strip undergoing flutter in a wind tunnel. This simplistic design provides a useful baseline not only for how much power a strip of IPMC can produce, but also an insight into what to expect from an array of multiple IPMC strips for a greater power output. The authors hope that data presented also provide a helpful reference for fluid–structure simulations required for a comprehensive analysis of the energy harvesting potential of flexible electro-active devices. Energy harvesting circuit optimization is not a subject of the current research.

Fig. 1 Ionic polymer–metal composite used in experiments

2 Materials and Methods

2.1 Material Overview. Ionic polymer–metal composites are a type of flexible electro-active polymer within the class of smart materials. They consist of an electro-active ionic polymer, sandwiched between two noble metal electrodes. The noble metal electrodes are formed in a two-step process: the initial compositing process and the surface electroding process. The IPMC used in this study consists of a Nafion 117 ionic polymer and platinum surface electrodes. The dimensions of the IPMC strip utilized in the experiments are $0.1\,\mathrm{m} \times 8 \times 10^{-3}$ m $\times 2 \times 10^{-4}$ m (Fig. 1). Thickness of each platinum electrode is 13×10^{-6} m as reported by the manufacturer.[2]

As an electro-active material, IPMC can act as a sensor or as an actuator. If a time-varying electric field is applied across the surface electrodes, the IPMC will deform. Conversely, if the IPMC is subject to quasi-static or dynamic deformation, a charge difference between its electrodes will occur. This differential charge can be measured from differential voltage between the two electrodes. The magnitude of this differential voltage is directly proportional to the mechanical deformation input [1].

The charge gradient formed in an ionic polymer is due to the ion transport and the electrophoretic solvent transport [1]. In our study, de-ionized (DI) water was used as an electrophoretic solvent. A defining property of ionic polymers is that ions with one charge are fixed, and ions of the opposite charge are mobile. In Nafion 117, anions are fixed to the polymeric structure in the whole volume; sodium cations are mobile. The role of an electrophoretic solvent is to hydrate the sodium cations creating $Na(H_2O)_4+$. When a bending deformation is applied to IPMC, the hydrated cations are forced away from the compressed side of the beam creating a net positive charge on the side of the beam in tension. This charge accumulates on the platinum electrode at the IPMC surfaces and can be measured by the difference in voltage between the two electrodes as mentioned above. As with any capacitive system, the charge tends to disperse back to an equilibrium state, and therefore, dynamic deformation of IPMC is required for energy harvesting.

With such a thin beam made up mostly of the Nafion 117 membrane, the elastic modulus of IPMC is low: between 30 and 60 MPa [12]. That is, very large deformations of this material can be achieved in actuation with small voltages (In general, IPMCs have larger actuation displacement and lower reaction speed than other smart material such as shape memory alloys, for example).

[2]Environmental Robots Incorporated, Bangor, ME.

The low elastic modulus also makes the material sensitive to ambient vibrations, which is beneficial for harvesting energy from wind. Moreover, IPMCs are resilient and elastic in terms of fracture toughness [4].

2.2 Experimental Setup and Procedure. In our experiments, the IPMC strip was tested in an Engineering Laboratory Design Inc. 401 open-circuit 0.35 HP (horsepower) subsonic wind tunnel (Fig. 2(*a*)) located at the Department of Mechanical Engineering, University of New Mexico. The strip was mounted at the top of the tunnel 6-in. square test section, as shown in Fig. 2(*b*). A custom insert was designed and fabricated in-house to minimize roughness along the top of the test section. Each trial was carried out immediately following complete hydration of IPMC in the DI water. This was done to ensure that the IPMC strip retained electrical and mechanical properties throughout the data collection period.

The IPMC strip was clamped between two copper electrodes. The clamp, shown in Fig. 3, was constructed in-house, and the surfaces of the electrodes were sanded periodically to ensure full contact with the IPMC surface.

The short-circuit current from the IPMC strip was delivered to a current-to-voltage converter employing a TL082 operational amplifier. The converter was calibrated to a current-to-voltage gain of 1 V/1 mA following the converter designed in Ref. [17]. A National Instruments USB-5132 digitizer, with a sampling frequency range of 763 Hz to 50 MHz, was used to measure the resulting voltage. Measured voltages were then converted to currents using the current-to-voltage gain measured above.

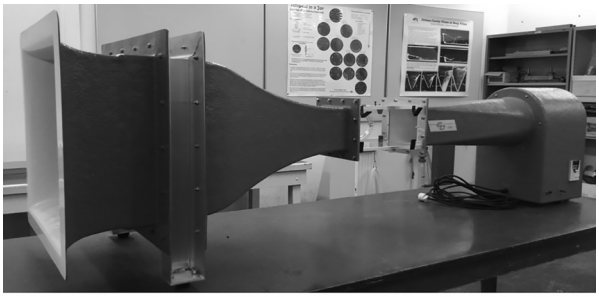

(*a*)

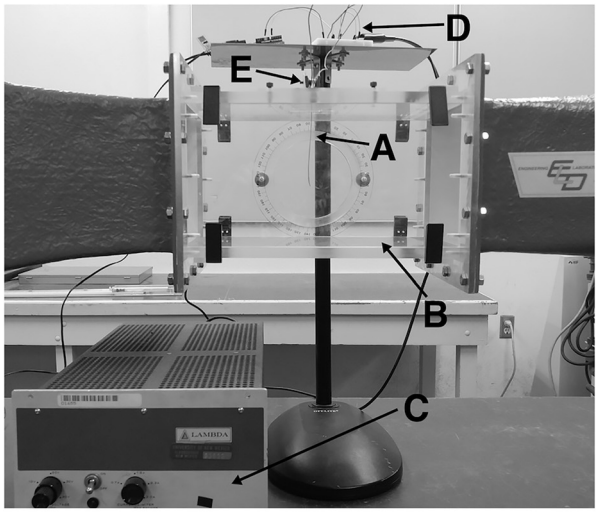

(*b*)

Fig. 2 Experimental setup: (*a*) wind tunnel and (*b*) the tunnel enlarged test section. Notations: (A) the IPMC strip, (B) the wind tunnel test chamber, (C) the power supply, (D) the TL02 operational amplifier for current-to-voltage conversion, and (E) the electrode-plated clamp.

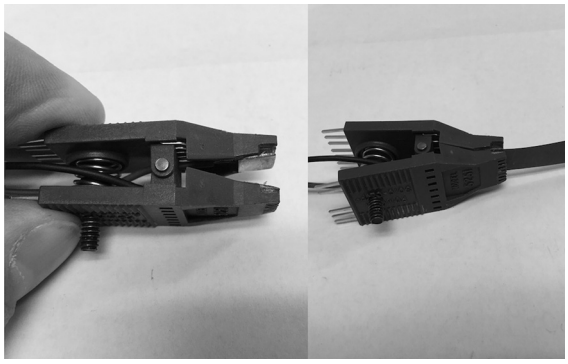

Fig. 3 Clamp used to secure IPMC strip. On the left, the clamp is shown opened to display the copper electrodes. The clamp is shown closed on the right, holding the IPMC strip.

Experiments in the wind tunnel were conducted at air speeds from 5.41 m/s to 6.80 m/s. Flutter was neither observed visually nor manifested electrically at wind speeds below 5.41 m/s. Above 6.80 m/s, the IPMC strip behavior became erratic and less repeatable, which made it challenging for data collection and analysis.

The air speed values were obtained using the manufacturer calibration data and appropriate frequency values for the variable frequency drive (VFD, inverter) driving the electric motor powering the wind tunnel, with resulting uncertainty in air speed not exceeding 2.5% of the value.

In experiments, the wind tunnel VFD frequency values were incremented by 0.5 Hz, which resulted in 11 air speeds in the range from 5.41 m/s to 6.80 m/s. Thirty experiments (hereafter, trials) were conducted at each speed to obtain a statistically meaningful dataset. During each trial, the current amplitude was measured as a function of time.

In the context of flutter analysis, frequencies that get excited by the flow are of particular interest. Therefore, the data collected at the previous step were then converted into the frequency domain using the fast Fourier transform in MATLAB [47].

2.3 Postprocessing Scheme. Data output from the IPMC strip was sampled at a frequency of 200 kHz for a period of 0.5 s per experimental trial. When data were collected for longer than 0.5 s periods of to time, a significant reduction in performance was observed, likely due to the DI water evaporation.

All postprocessing was performed using a MATLAB program tailored to experimental conditions. A median filter and a moving average filter with a center frequency of 180 Hz were applied to the raw data to eliminate high-frequency noise produced by the IPMC. Zero offset correction was then performed.

The maximum (or peak) current amplitude in each trial was recorded, and the fast Fourier transform was performed to convert the data from the time domain to the frequency domain in order to determine the primary flutter frequency for each trial. The primary flutter frequency averaged over 30 trials at each wind velocity was taken as the primary flutter frequency at that air speed.

The data were further processed by isolating a single period of flutter defined by the average of maximum and minimum primary flutter frequencies recorded in the range of considered air speeds. Flutter characteristics will be discussed in more detail in Sec. 3.

The charge accumulated on the IPMC strip during one flutter period was then found by integrating the short-circuit current versus time curve using a trapezoidal approximation. Finally, the amount of energy transduced by the IPMC strip during one flutter period was estimated using the IPMC capacitance, which was measured directly using a digital multimeter. Results and additional details of this postprocessing procedure are presented in Sec. 3.

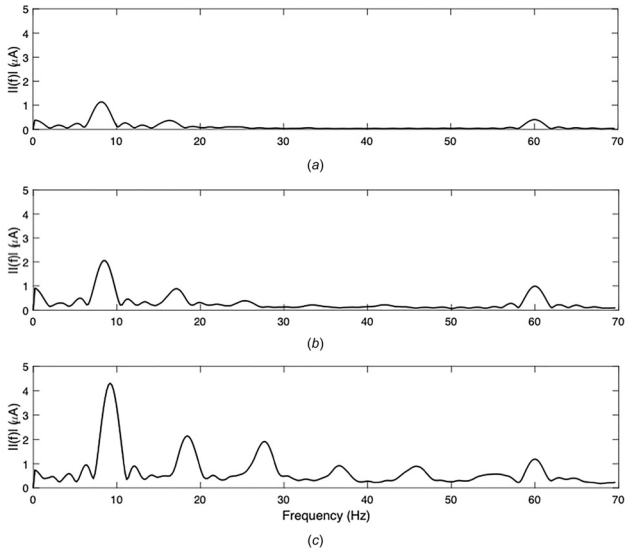

Fig. 4 Averaged current amplitude (in μA) in the frequency domain generated by the IPMC strip at three air speeds: (*a*) 5.41 m/s, (*b*) 6.10 m/s, and (*c*) 6.80 m/s

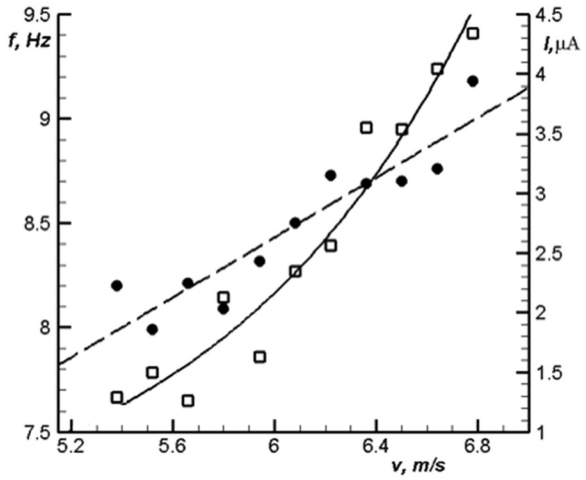

Fig. 5 Averaged peak current amplitude I (in μA) (open squares) and the flutter frequency (in Hz) (solid circles) at different air speeds. Solid and dashed lines are exponential and linear fitting lines for the data.

3 Results and Discussion

Figure 4 shows the current amplitude as a function of frequency, |I(f)|, averaged over 30 trials at three values of the air speed: 5.41, 6.10, and 6.80 (in m/s), as an example. Note that peaks near 60 Hz can likely be attributed to the instrument noise, a phenomenon supported by control testing. The plot only shows frequencies up to 70 Hz because signals above this frequency were completely attenuated by the signal processing scheme.

The figure demonstrates that at the lowest air speed of 5.41 m/s at which the IPMC strip flutter was detected, the peak current amplitude is 1.29×10^{-6}A at the primary flutter frequency of 8.2 Hz. The peak current amplitude and the frequency at which it is observed increase with the air speed growth: 2.35×10^{-6}A at 8.5 Hz at the air speed of 6.10 m/s and 4.34×10^{-6} A at 9.18 Hz at the air speed of 6.80 m/s.

Figure 5 and Table 1 provide data for the averaged primary flutter frequency (solid circles) and the corresponding averaged current amplitude (open squares) for all considered values of the air speed. Observed increase in the primary flutter frequency from 8.2 to 9.18 Hz can be approximated as linear (dashed line in Fig. 5), whereas the increase in the peak current amplitude is exponential (solid line in Fig. 5).

The charge accumulated on the IPMC strip was estimated by integrating the short-circuit current versus time curve over one period of flutter. Its value was assumed to be constant for all considered air speeds in order to keep the total integration time constant for comparison. The primary flutter frequency of 8.585 Hz—the average of maximum and minimum primary flutter frequencies from Table 1—was used to determine this flutter period. Integration was conducted using a trapezoidal approximation in MATLAB [47].

After the charge values for each trial were calculated, outliers in the data were eliminated from each sample. A data point was defined as an outlier if it fell more than three standard deviations outside of the sample mean at a specific wind velocity.

Finally, power transduced during the flutter period in each trial was estimated by modeling the IPMC reactive behavior as a simple capacitor using the following relation:

$$P_{\text{IPMC}} = \frac{Q_{\text{IPMC}}^2}{2tC_{\text{IPMC}}} \tag{1}$$

where Q_{IPMC} is the charge, C_{IPMC} is the capacitance of the IPMC strip, and t is the time duration of the flutter period [17].

The capacitance value of 30.8 mF was measured using a digital multimeter. The mean and standard deviation of these power values were computed for each 30-trial sample and are provided in Table 1. The mean power data can be fitted by a second-order polynomial curve obtained by using the least-squares based method in MATLAB [47]. Data for the power transduced in individual trials and the curve fit for the mean power values are shown in Fig. 6 by symbols and the solid line, respectively.

Data obtained in this study have uncertainties associated with them, with some of them being unique for the IPMC strip used. In particular, fluttering makes the material susceptible to residual stresses and fatigue with time, which affects measurements. Such information was not available to us during the project lifetime but poses an interesting research question for future studies.

Another contributor in the data uncertainty is hydration of the IPMC strip. Specifically, the IPMC level of hydration affects the IPMC bending stiffness, degree of deformation, and as a result, the measured short-circuit current. In our study, all experiments were performed immediately after the IPMC strip hydration. However, random errors associated with the procedure are inevitable. Also, we could not find information in literature about how quickly IPMCs dehydrate in airflow and how this process may affect measurements.

The capacitance measurement may be a significant source of error in the power data presented in Table 1 as the method by which the capacitance was measured in this study produced a value which was several orders of magnitude higher than the approximate specification given by the manufacturer (in the microfarad range). Further studies are required to clarify this issue.

Digital signal processing may also have introduced an error into the data due to the nature of the filters used. The error due to signal processing is systematic as the same filtering scheme was applied to all data, but signal processing could have caused an underestimation of peak current and total power transduced per flutter period.

A random error may also be attributed to the clamping of the IPMC strip as this was done manually for each experimental trial, and no device was instituted to make sure that the IPMC strip was clamped exactly in the same fashion every time.

Regarding the aforementioned sources of possible error, it is believed that the experimental procedure of running 30 trials for each air speed tested produced a viable field of data from which to

Table 1 Key quantities related to power transduction during IPMC flutter

Air speed (m/s)	Primary flutter frequency, f_0 (Hz)	Average current amplitude at f_0 (μA)	Mean power transduced per the flutter period (μW)	Standard deviation (μW)
5.41	8.20	1.29	1.20	0.90
5.55	7.99	1.50	1.68	1.24
5.69	8.21	1.26	1.20	0.82
5.83	8.09	2.13	2.50	1.88
5.96	8.32	1.63	2.16	1.34
6.10	8.50	2.35	4.40	2.10
6.24	8.73	2.56	3.98	1.68
6.38	8.69	3.55	14.96	5.98
6.52	8.70	3.54	14.52	5.82
6.66	8.76	4.04	17.76	2.10
6.80	9.18	4.34	22.94	1.68

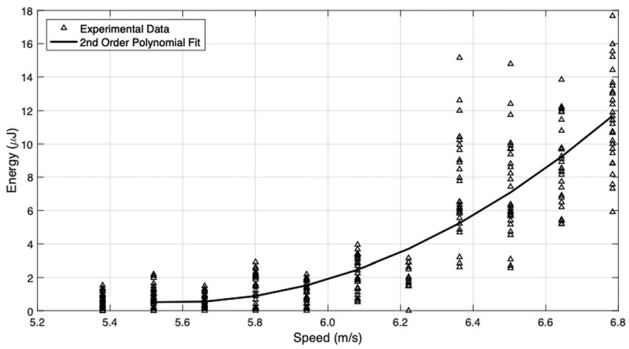

Fig. 6 Energy harvested from the IPMC strip over one flutter period. The solid line shows the second-order polynomial fit for the mean energy values. Note that the wider distribution of data points at higher wind speeds is due to the increased chaotic motion of the device.

produce reliable averaging. As such, reproduction of the experiment presented herein should yield similar results.

Finally, follow-up experiments were conducted with the same strip one year later after the experiments described above were completed, to determine the IPMC ability to preserve its electro-active properties in time when kept in storage under local atmospheric conditions. The testing demonstrated that the strip electro-active properties completely deteriorated, which implies that this material has an overall finite time period in which it can be utilized. Further studies are required to clarify this issue.

To summarize, the data provided in Table 1 have to be viewed as a proof of concept that flexible electro-active devices can be utilized on their own (as stand-alone devices) for energy harvesting using a naturally occurring phenomenon such as flutter. The IPMC outputs can further be improved by optimizing manufacturing process of the IPMC device with the focus on energy harvesting and by assembling arrays of such devices. The small size of electro-active devices and the air speed range where flutter occurs create a specific niche for the potential use of such devices, that is, in urban residential areas in locations inaccessible for other renewable energy technologies. Indeed, wind speeds in residential areas are typical of those shown in Table 1 [48]. These wind speeds are also not of great harvesting potential from the perspective of the traditional wind turbine industry [49].

4 Conclusion

In this paper, a possibility of utilizing a flexible electro-active polymer such as IPMC for harvesting wind energy as a stand-alone device has been explored. Specifically, the behavior of a thin rectangular strip of IPMC in a low-velocity air flow was studied. Experiments were conducted in the open-circuit wind tunnel at the Department of Mechanical Engineering, University of New Mexico. It has been detected that the IPMC strip undergoes flutter in the range of air speed from 5.41 m/s to 6.80 m/s and thus can potentially be used as a wind harvesting device. The flutter frequency shows insignificant increase with the growth of air speed, whereas the peak current amplitude grows exponentially in the considered air speed range. From a practical perspective, arrays of IPMC strips have more potential than stand-alone devices due to the small power generated by a single strip. However, the small size of such devices and their high responsiveness to low wind speeds make them a particularly good candidate for energy harvesting in places inaccessible for other renewable energy technologies or in combination with them in urban areas, for example, where wind speeds are typically within the speed range where the IPMC strip experiences flutter. More studies are required to fully comprehend how the device power output, durability, and longevity can be enhanced, and the production cost reduced. Further studies will also be necessary to maximize power output from this device and to increase its commercial viability. A connection between the IPMC sample geometry and its viability in array settings has also yet to be established.

Acknowledgment

Gary Macias helped with manufacturing the clamping mechanism for the IPMC device. Dr. Dell Olmstead provided help with electronics and experimental setup.

Funding Data

- University of New Mexico (UNM) Women in Stem (WIS) Faculty Development Fund (Funder ID: 10.13039/100007179).
- National Science Foundation EPSCoR (OIA-1757207).

Nomenclature

C_{IPMC} = capacitance of IPMC strip
f_{vfd} = frequency setting on variable frequency drive
f_0 = primary flutter frequency
$|I(f)|$ = amplitude of current
IPMC = ionic polymer–metal composite
P_{IPMC} = power transduced by IPMC strip
Q_{IPMC} = charge of IPMC strip
v = wind velocity
VFD = variable frequency drive

References

[1] Shahinpoor, M., and Kim, K. J., 2001, "Ionic Polymer-Metal Composites: I—Fundamentals," Smart Mater. Struct., **10**(4), pp. 819–833.
[2] Kim, K. J., and Shahinpoor, M., 2003, "Ionic Polymer–Metal Composites: II—Manufacturing Techniques," Smart Mater. Struct., **12**(1), pp. 65–79.

[3] Shahinpoor, M., and Kim, K. J., 2004, "Ionic Polymer–Metal Composites: III—Modeling and Simulation as Biomimetic Sensors, Actuators, Transducers, and Artificial Muscles," Smart Mater. Struct., **13**(6), pp. 1362–1388.
[4] Shahinpoor, M., and Kim, K. J., 2005, "Ionic Polymer–Metal Composites: IV—Industrial and Medical Applications," Smart Mater. Struct., **14**(1), pp. 197–214.
[5] Chen, Z., Tan, X., Will, A., and Ziel, C., 2007, "A Dynamic Model for Ionic Polymer–Metal Composite Sensors," Smart Mater. Struct., **16**(4), pp. 1477–1488.
[6] Branco, P. J. C., and Dente, J. A., 2006, "Derivation of a Continuum Model and Its Electric Equivalent-Circuit Representation for Ionic Polymer–Metal Composite (IPMC) Electromechanics," Smart Mater. Struct., **15**(2), pp. 378–392.
[7] Lee, S., Park, H. C., and Kim, K. J., 2005, "Equivalent Modeling for Ionic Polymer–Metal Composite Actuators Based on Beam Theories," Smart Mater. Struct., **14**(6), pp. 1363–1368.
[8] Simpson, J., Lumia, R., and Martinez, M., 2013, "Force and Deflection Modeling of IPMC Fingers," Tenth IEEE International Conference on Networking, Sensing and Control (ICNSC), Evry, France, Apr. 10–12, pp. 136–140.
[9] Jung, K., Nam, J., and Choi, H., 2003, "Investigations on Actuation Characteristics of IPMC Artificial Muscle Actuator," Sens. Actuators A, **107**(2), pp. 183–192.
[10] Aureli, M., 2012, "Multiphysics Modeling of Ionic Polymer Metal Composites for Underwater Applications," Polytechnic Institute of New York University, New York, accessed Apr. 4, 2020, http://search.proquest.com/dissertations/docview/1034436555/abstract/D5416BA3E4A24AF0PQ/1?accountid=14613
[11] Dias, J. A. C., De Marqui, C., and Erturk, A., 2013, "Hybrid Piezoelectric-Inductive Flow Energy Harvesting and Dimensionless Electroaeroelastic Analysis for Scaling," Appl. Phys. Lett., **102**(4), p. 044101.
[12] Tiwari, R., and Garcia, E., 2011, "The State of Understanding of Ionic Polymer Metal Composite Architecture: A Review," Smart Mater. Struct., **20**(8), p. 083001.
[13] Brufau-Penella, J., Puig-Vidal, M., Giannone, P., Graziani, S., and Strazzeri, S., 2008, "Characterization of the Harvesting Capabilities of an Ionic Polymer Metal Composite Device," Smart Mater. Struct., **17**(1), p. 015009.
[14] Tiwari, R., and Kim, K. J., 2013, "IPMC as a Mechanoelectric Energy Harvester: Tailored Properties," Smart Mater. Struct., **22**(1), p. 015017.
[15] Peterson, S. D., and Porfiri, M., 2012, "Energy Exchange Between a Vortex Ring and an Ionic Polymer Metal Composite," Appl. Phys. Lett., **100**(11), p. 114102.
[16] Aureli, M., Prince, C., Porfiri, M., and Peterson, S. D., 2010, "Energy Harvesting From Base Excitation of Ionic Polymer Metal Composites in Fluid Environments," Smart Mater. Struct., **19**(1), p. 015003.
[17] Aureli, M., Lin, W., and Porfiri, M., 2009, "On the Capacitance-Boost of Ionic Polymer Metal Composites Due to Electroless Plating: Theory and Experiments," J. Appl. Phys., **105**(10), p. 104911.
[18] Cellini, F., Cha, Y., and Porfiri, M., 2014, "Energy Harvesting From Fluid-Induced Buckling of Ionic Polymer Metal Composites," J. Intell. Mater. Syst. Struct., **25**(12), pp. 1496–1510.
[19] Cellini, F., Pounds, J., Peterson, S. D., and Porfiri, M., 2014, "Underwater Energy Harvesting From a Turbine Hosting Ionic Polymer Metal Composites," Smart Mater. Struct., **23**(8), p. 085023.
[20] Cha, Y., Verotti, M., Walcott, H., Peterson, S. D., and Porfiri, M., 2013, "Energy Harvesting From the Tail Beating of a Carangiform Swimmer Using Ionic Polymer–Metal Composites," Bioinspir. Biomim., **8**(3), p. 036003.
[21] Shafer, M. W., Bryant, M., and Garcia, E., 2012, "Designing Maximum Power Output Into Piezoelectric Energy Harvesters," Smart Mater. Struct., **21**(8), p. 085008.
[22] Sodano, H. A., Park, G., and Inman, D. J., 2004, "Estimation of Electric Charge Output for Piezoelectric Energy Harvesting," Strain, **40**(2), pp. 49–58.
[23] Sodano, H. A., Inman, D. J., and Park, G., 2005, "Generation and Storage of Electricity From Power Harvesting Devices," J. Intell. Mater. Syst. Struct., **16**(1), pp. 67–75.
[24] Cha, Y., Kim, H., and Porfiri, M., 2014, "Matching the Impedance of Ionic Polymer Metal Composites for Energy Harvesting," Smart Mater. Struct., **23**(12), p. 127002.
[25] Eloy, C., Lagrange, R., Souilliez, C., and Schouveiler, L., 2008, "Aeroelastic Instability of Cantilevered Flexible Plates in Uniform Flow," J. Fluid Mech., **611**, pp. 97–106.
[26] Epureanu, B. I., Tang, L. S., and PaïDoussis, M. P., 2004, "Coherent Structures and Their Influence on the Dynamics of Aeroelastic Panels," Int. J. Non-Linear Mech., **39**(6), pp. 977–991.
[27] Jamshidi, S., Dardel, M., Pashaei, M. H., and Alashti, R. A., 2015, "Energy Harvesting From Limit Cycle Oscillation of a Cantilever Plate in Low Subsonic Flow by Ionic Polymer Metal Composite," Proc. Inst. Mech. Eng., Part G, **229**(5), pp. 814–836.
[28] Shelley, M., Vandenberghe, N., and Zhang, J., 2005, "Heavy Flags Undergo Spontaneous Oscillations in Flowing Water," Phys. Rev. Lett., **94**(9), p. 094302.
[29] Akcabay, D. T., and Young, Y. L., 2012, "Hydroelastic Response and Energy Harvesting Potential of Flexible Piezoelectric Beams in Viscous Flow," Phys. Fluids (1994-Present), **24**(5), p. 054106.
[30] Alben, S., 2008, "The Flapping-Flag Instability as a Nonlinear Eigenvalue Problem," Phys. Fluids (1994-Present), **20**(10), p. 104106.
[31] Sirohi, J., and Mahadik, R., 2011, "Piezoelectric Wind Energy Harvester for Low-Power Sensors," J. Intell. Mater. Syst. Struct., **22**(18), pp. 2215–2228.
[32] Giacomello, A., and Porfiri, M., 2011, "Underwater Energy Harvesting From a Heavy Flag Hosting Ionic Polymer Metal Composites," J. Appl. Phys., **109**(8), p. 084903.
[33] Hobeck, J., and Inman, D., 2012, "Artificial Piezoelectric Grass for Energy Harvesting From Turbulence-Induced Vibration," Smart Mater. Struct., **21**(10), p. 105024.
[34] Fei, F., and Li, W. J., 2009, "A Fluttering-to-Electrical Energy Transduction System for Consumer Electronics Applications," IEEE International Conference on Robotics and Biomemetics (ROBIO), Guilin, China, Dec. 19–23, pp. 580–585.
[35] Perez, M., Boisseau, S., Geisler, M., Gasnier, P., Willemin, J., Despesse, G., and Reboud, J. L., 2018, "Aeroelastic Flutter Energy Harvesters Self-Polarized by Triboelectric Effects," Smart Mater. Struct., **27**(1), p. 014003.
[36] Ravichandran, A. N., Calmes, C., Serres, J. R., Ramuz, M., and Blayac, S., 2019, "Compact and High Performance Wind Actuated Venturi Triboelectric Energy Harvester," Nano Energy, **62**, pp. 449–457.
[37] Theodorsen, T., 1949, "General Theory of Aerodynamic Instability and the Mechanism of Flutter," National Advisory Committee for Aeronautics, Langley Aeronautical Lab., Langley Field, VA, Report No. NACA-TR-496.
[38] Farthing, S. P., 2013, "Binary Flutter as an Oscillating Windmill—Scaling & Linear Analysis," Wind Eng., **37**(5), pp. 483–499.
[39] Jin, Y., Kim, J.-T., Fu, S., and Chamorro, L. P., 2019, "Flow-Induced Motions of Flexible Plates: fluttering, Twisting and Orbital Modes," J. Fluid Mech., **864**, pp. 273–285.
[40] Fernandes, A. C., and Mirzaeisefat, S., 2015, "Flow Induced Fluttering of a Hinged Vertical Flat Plate," Ocean Eng., **95**, pp. 134–142.
[41] Eloy, C., Souilliez, C., and Schouveiler, L., 2007, "Flutter of a Rectangular Plate," J. Fluids Struct., **23**(6), pp. 904–919.
[42] Vedeneev, V. V., 2006, "High-Frequency Flutter of a Rectangular Plate," Fluid Dyn., **41**(4), pp. 641–648.
[43] Guo, C. Q., and Paidoussis, M. P., 2000, "Stability of Rectangular Plates With Free Side-Edges in Two-Dimensional Inviscid Channel Flow," ASME J. Appl. Mech, **67**(1), pp. 171–176.
[44] Chad Gibbs, S., Wang, I., and Dowell, E., 2012, "Theory and Experiment for Flutter of a Rectangular Plate With a Fixed Leading Edge in Three-Dimensional Axial Flow," J. Fluids Struct., **34**, pp. 68–83.
[45] Watanabe, Y., Suzuki, S., Sugihara, M., and Sueoka, Y., 2002, "An Experimental Study of Paper Flutter," J. Fluids Struct., **16**(4), pp. 529–542.
[46] Watanabe, Y., Isogai, K., Suzuki, S., and Sugihara, M., 2002, "A Theoretical Study of Paper Flutter," J. Fluids Struct., **16**(4), pp. 543–560.
[47] MathWorks, "MATLAB Documentation," accessed Apr. 7, 2020, https://www.mathworks.com/help/matlab/index.html?s_tid=gn_loc_drop
[48] Heisler, G. M., 1990, "Mean Wind Speed Below Building Height in Residential Neighborhoods With Different Tree Densities," ASHRAE Trans., **96**(1), pp. 1389–1396.
[49] U.S. Department of Energy, 2020, "Enabling Wind Power Nationwide," Oak Ridge, TN, accessed Apr. 4, 2020, https://www.energy.gov/sites/prod/files/2015/05/f22/Enabling%20Wind%20Power%20Nationwide_18MAY2015_FINAL. pdf